OPEN ACCESS Freely available online

PLOS ONE

Primed Infusion with Delayed Equilibrium of Gd.DTPA for Enhanced Imaging of Small Pulmonary Metastases

Tammy L. Kalber[1,2]*, Adrienne E. Campbell-Washburn[1], Bernard M. Siow[1], Elizabeth Sage[2], Anthony N. Price[1], Katherine L. Ordidge[1,2], Simon Walker-Samuel[1], Sam M. Janes[2¶], Mark F. Lythgoe[1¶]

1 UCL Centre of Advanced Biomedical Imaging, Division of Medicine and Institute of Child Health, University College London, London, United Kingdom, **2** Centre for Respiratory Research, Department of Medicine, University College London, London, United Kingdom

Abstract

Objectives: To use primed infusions of the magnetic resonance imaging (MRI) contrast agent Gd.DTPA (Magnevist), to achieve an equilibrium between blood and tissue (eqMRI). This may increase tumor Gd concentrations as a novel cancer imaging methodology for the enhancement of small tumor nodules within the low signal-to-noise background of the lung.

Methods: A primed infusion with a delay before equilibrium (eqMRI) of the Gd(III) chelator Gd.DTPA, via the intraperitoneal route, was used to evaluate gadolinium tumor enhancement as a function of a bolus injection, which is applied routinely in the clinic, compared to gadolinium maintained at equilibrium. A double gated (respiration and cardiac) spin-echo sequence at 9.4T was used to evaluate whole lungs pre contrast and then at 15 (representative of bolus enhancement), 25 and 35 minutes (representative of eqMRI). This was carried out in two lung metastasis models representative of high and low tumor cell seeding. Lungs containing discrete tumor nodes where inflation fixed and taken for haematoxylin and eosin staining as well as CD34 staining for correlation to MRI.

Results: We demonstrate that sustained Gd enhancement, afforded by Gd equilibrium, increases the detection of pulmonary metastases compared to bolus enhancement and those tumors which enhance at equilibrium are sub-millimetre in size (<0.7 mm^2) with a similar morphology to early bronchoalveolar cell carcinomas.

Conclusion: As Gd-chelates are routinely used in the clinic for detecting tumors by MRI, this methodology is readily transferable to the clinic and advances MRI as a methodology for the detection of small pulmonary tumors.

Citation: Kalber TL, Campbell-Washburn AE, Siow BM, Sage E, Price AN, et al. (2013) Primed Infusion with Delayed Equilibrium of Gd.DTPA for Enhanced Imaging of Small Pulmonary Metastases. PLoS ONE 8(1): e54903. doi:10.1371/journal.pone.0054903

Editor: Vladimir V. Kalinichenko, Cincinnati Children's Hospital Medical Center, United States of America

Received August 10, 2012; **Accepted** December 17, 2012; **Published** January 31, 2013

Funding: The main funding for this study was provided by the Nanotech Grand Challenge Engineering and Physical Sciences Research Council (EPSRC) grant (EP/G06262072/1 - http://www.epsrc.ac.uk), the British Heart Foundation, the King's College London and University College London Comprehensive Cancer Imaging Centre CR-UK & EPSRC, in association with the Medical Research Council (MRC) and Department of Health (England), and a Medical Research Council Capacity Building Studentship (KLO). This study was partly undertaken at UCLH/UCL who received a proportion of funding from the Department of Health's NIHR Biomedical Research Centres funding scheme. SMJ is a Wellcome Trust Senior fellow in Clinical Science (WT091730MA). The funders had no role in study design, data collection and analysis, decision to publish, or preparation of the manuscript.

Competing Interests: The authors have declared that no competing interests exist.

* E-mail: t.kalber@ucl.ac.uk

¶ These authors are joint senior authors on this work.

Introduction

Lung cancer is the commonest cause of cancer death worldwide with 152,000 deaths each year in the US (NCI 2011). Accurate and cost effective screening methods for lung cancer are desperately needed. Screening should be sensitive to small nodules, specific to the disease, able to detect suitability of patients for radical treatments and be non-invasive. Prior screening trials with chest radiographs have not found a reduction in lung cancer mortality [1,2,3]. Computer tomography (CT) is more sensitive than chest radiography and has recently been shown to be effective at reducing lung cancer mortality, although the feasibility and cost effectiveness of mass CT screening is still disputed [4,5,6]. CT imaging can detect pulmonary nodules as small as 2 to 3 mm, but current guidelines deem these small lesions clinically insignificant [7]. It also lacks the specificity to distinguish between benign and cancerous tumors, and nodules of 4 to 10 mm are followed up by repeated CT scans thereby increasing radiation burden [8].

Positron emission tomography (PET) with fluorodeoxyglucose is superior to CT in differentiating between malignant and benign tumors [9,10]. Preoperative use of PET has led to a reduction in the number of unnecessary thoracotomies in patients considered to be operable on the basis of CT criteria [11,12]. However PET has a low spatial resolution and reduced specificity for nodules smaller than 10 mm [13]. Further, specificity of PET in nodules larger than 10 mm can fall as low as 60% [14].

Magnetic resonance imaging (MRI) offers distinct advantages over both CT and PET as it uses non-ionising radiation and has better anatomical resolution in most tissues [15]. Lung imaging however is challenging for MRI, due to its low tissue density, many air-tissue interfaces, as well as respiratory and cardiac motion

artefacts, and thus it has not reached mainstream clinical use [16,17].

Gadolinium(III) (Gd) chelates have been widely used to detect and investigate functional tumor perfusion by MRI in other organs [18,19]. Gd-chelates are small molecules with short half lives, which leak out of capillaries into the interstitial space. Tumor blood vessels are a chaotic network of thin-walled leaky vessels leading to increased accumulation and retardation of wash out of Gd within viable tumor tissue termed the enhanced permeability and retention (EPR) effect [20,21]. As Gd-chelates are normally given as a single bolus, poorly vascularised tumors such as very small pre-angiogenic tumors may have limited enhancement [22]. However, studies combining bolus with subsequent infusion show that Gd concentrations in tissues of differing permeabilities can be increased [23]. Although the use of gadolinium for dynamic contrast enhancement (DCE) has had limited use in lung tumor imaging [24], it is conceivable that using a primed infusion, an equilibrium of Gd concentration between the vasculature and the interstitial spaces can be reached and sustained. This technique has been termed eqMRI and has been utilised to image myocardial fibrosis in humans [25], as well as systemic amyloidosis in preclinical murine models [26]. We hypothesised this technique may therefore improve the imaging of small lung tumors where equilibrium can provide continuous high concentrations of Gd enhancement.

In this study, primed infusions with a delay before equilibrium (eqMRI) of the Gd(III) chelator Gd.DTPA (Magnevist) were used to evaluate gadolinium tumor enhancement as a function of a bolus injection, which is applied routinely in the clinic, compared to gadolinium maintained at equilibrium. This was carried out in two lung metastasis models representative of high and low tumor cell seeding. We demonstrate that eqMRI specifically improves the detection of small pulmonary metastases compared to bolus enhancement. This methodology would be readily transferable to the clinic using a similar strategy to that used by Flett A.S. et al. in humans [25] and advances MRI as a methodology for the detection of small primary or metastatic tumors.

Materials and Methods

Tissue Culture

Cells were grown in T175 flasks (Fisher Scientific, Loughborough, UK) in Dulbecco's Modified Eagles Medium (DMEM) (Invitrogen, Paisley, UK), supplemented with 10% heat inactivated fetal calf serum (GIBCO, Grand Island NY, USA) in a humidified incubator at 37°C with 95% air, and 5% CO_2.

Lentiviral Production and Cell Transduction

Lentivirus vectors pseudotyped with the vesicular stomatitis G protein (VSV-G) were generated by transfection into 293T human kidney cells (ATCC) of a packaging construct (pCpr-ENV), a plasmid producing the VSV-G envelope (pVSV-G) and the vector encoding yellow fluorescent protein (YFP) and the luciferase gene (*Luc)* (pLIONII-HYG-Luc2YFP) as described previously [27]. Plasmid vectors were kindly provided by Dr S Goldie (Cancer Research Institute, CRUK, Cambridge UK). Conditioned medium was harvested at 24 hours and passed through 0.45 mm filters. The transduction of non-confluent MDA-MB-231 cells (CRUK) in a T175 flask was performed using 4 mg/ml polybrene (20 µl polybrene with 20 µl virus in 20 ml medium). The lentivirus was left for 48 hours before changing media. 24 hours later the presence of YFP was assessed by fluorescent microscopy. As the luciferase lentivirus contains a hygromycin resistance gene, 200 µg/ml Hygromycin B was added to culture media for 48 hours. Cells were found to be 96% transfected by flow cytometry using a FACS Calibur (Becton Dickinson, Franklin Lakes NJ, USA).

Animal Model

All animal studies were approved by the University College London Biological Services Ethical Review Committee and licensed under the UK Home Office regulations and the Guidance for the Operation of Animals (Scientific Procedures) Act 1986 (Home Office, London, United Kingdom). Animal weights were recorded every two days and tumor monitoring was carried out weekly by bioluminescence and MRI scanning with animal monitoring equipment. All procedures were carried out under breathing anaesthesia. Mice were sacrificed with 200 µl pentobarbital by intraperitoneal (i.p) injection (200 mg/ml) and death was confirmed by exsanguination prior to lung inflation (see histology). Male NOD SCID gamma (NSG) mice, 6–8 weeks, were anaesthetised using 2% isoflurane and the tail vein cannulated for infusion of cells. Mice either received a high seeding of cells (2×10^6 cells in 200 µl serum free media, n = 6, 3 eqMRI & 3 high dose) to achieve rapid growing multiple metastases for weekly longitudinal evaluation, or a low seeding of cells (1×10^5 cells in 200 µl serum free media, n = 3) to produce slower growing discrete nodules. These low seeding tumors were taken for histology as soon as they were identified by MRI. Control mice received no cells. Mice were imaged using bioluminescence directly after injection and then by both bioluminescence and MRI at weekly time points.

Bioluminescence Imaging

Mice were anesthetized with 2% isoflurane before and during imaging. An aqueous solution of D-luciferin (Regis Technologies Inc, Morton Grove, IL, USA) at 150 mg/kg in a volume of 200 µl was injected i.p 10 minutes before imaging. Imaging was performed using an IVIS® Lumina II bioluminescent scanner (Caliper Life Sciences, Hopkinton, MA, USA). Quantification of the bioluminescent signal was performed using a region of interest (ROI) covering the whole thorax using Living Image software (version 4: Caliper Life Sciences).

eqMRI

Mice were anesthetized with 2% isoflurane before and during imaging. Two i.p lines were used to administer either a bolus or an infusion of Gd.DTPA (Magnevist®, Schering, Berlin). Although, the kinetics of intravenous and i.p injection is different once equilibrium is reached the steady state is the same [26]. For this purpose the i.p route is more suitable and the dosing has been based on the late Gd i.p mouse dose described by Price A.N *et al.*2011 [28] with the subsequent infusion half the bolus dose over 1 hour as described for eqMRI by Campbell A.E *et al.* 2011 [26]. Imaging was performed on an Agilent 9.4T scanner (Agilent Technologies. Santa Clara, CA, USA) with a 39 mm coil (RAPID Biomed, Rimpar, Germany) using a multi-slice double gated (respiration and cardiac) spin-echo sequence with the following parameters: TR ~ 3.6 s (between RF TR 120–150 ms) determined by gating and number of slices (breathing rate ~ 50 breaths/minute, and heart rate 400–500 beats/minute), TE = 9.6 ms, FOV = 30×30 mm (3×3 cm), averages = 1: matrix size = 256×128, slices = 10, thickness = 1 mm. Scan time ~ 8 minutes. After the initial pre contrast scan, mice were given a bolus of 0.6 mmol/kg Gd.DTPA (prime) and after 15 minutes an infusion of 0.005 mmol/kg/min Gd.DTPA was started. Images were acquired directly after the infusion was started at 15 minutes, synonymous with tumor enhancement from the bolus only

(preliminary bolus experiments showed this to be the maximal enhancement in subcutaneous tumors via i.p). Images were acquired again at both 25 and 35 minutes, equivalent to tumor enhancement caused by Gd equilibrium in normal tissues (Figure 1). This methodology of bolus with delayed infusion allows for direct comparison of tumor enhancement following bolus compared to equilibrium.

eqMRI vs High Dose

To assess if tumor enhancement at 25 minutes onwards was due to Gd equilibrium and not just the increased dose of Gd, the total dose of Gd.DTPA for eqMRI was given as a single bolus dose (high dose) in three mice at day 14 (high tumor seeding mice) and compared to eqMRI at the same imaging time points (Figure 1).

MRI Data Analysis

Signal-to-noise (Figure S1). All images were analysed using ImageJ (Rasband, ImageJ, U.S. National Institutes of Health, Bethesda, Maryland, USA, http://rsb.info.nih.gov/ij/, 1997–2008). Signal-to-noise ratios (SNR) for control lung were obtained from a ROI from whole lung (excluding major vessels) at each time point. To assess the enhancement in individual tumors, ROIs for SNR were drawn around a discrete lesion at the first point of tumor visualisation and then loaded onto the corresponding pre or post images to give the SNR time course for each tumor. Tumors were classed into two; either visible (detected without Gd) or enhancing (detectable after Gd only). In the low tumor cell seeding model, each mouse had one enhancing tumor (n = 3) and at least one visible tumor (n = 5) and a two-sample equal variance t-test was used. Whereas, in the high tumor cell seeding model, three enhancing and three visible tumors were chosen from each mouse (n = 9). Therefore a two-tailed paired t-test assuming equal variances was performed at each time point to determine significant difference, at the 5% level statistical significance.

Tumor volume measurements (Figure S2). To assess the increase in visualized tumors by Gd enhancement, an ROI was drawn around the whole lung (excluding major vessels) on each slice and the total lung volume calculated. As the signal intensity (SI) values of control lung were low, SI values above this threshold were deemed as either tumor or normal enhancing tissue. A threshold was applied from the highest SI value of control lung and the volume of the remaining tissue calculated as a percentage of the total lung volume. To account for the normal enhancing tissue the value obtained from control lung was subtracted from this as a correction value. The resulting volume left is therefore that of tumor and is termed the "percentage lung tumor volume". To assess if Gd equilibrium increased the number of tumors visible compared to bolus, the percentage lung tumor volume at 15, 25 and 35 minutes was divided by the pre contrast volume and expressed as a percentage increase, termed as the "percentage increase in observed tumors". A similar approach to assessing lung tumor burden has been described by Tidwell V.K *et al.* 2012 [29]. A two-tailed paired t-test assuming equal variances was performed at each time point to determine significant difference (n = 3 per group), at the 5% level statistical significance. Errors are given as standard errors of the mean (s.e.m) for both SNR and the percentage increase in observed tumors.

Histology

Inflated lungs were fixed in 4% formalin for 4 hours at 4°C and then incubated overnight in 15% sucrose in PBS at 4°C. Tissue was dehydrated in 70% ethanol and embedded in paraffin. Sections corresponding to MR images were cut at 5 μm. Sections were stained with either Haematoxylin (Sigma-Aldrich, Dorset, UK) for 1 minute and Eosin (Sigma-Aldrich, UK) for 30 seconds (H & E), or by CD34 immunohistochemistry. Immunohistochemistry, including antigen retrieval and signal amplification was carried out as previously described [30]. Antibodies for CD34 detection were as follows; rat anti-mouse primary CD34 antibody at a 1:5 dilution (Hycult Biotech, The Netherlands), biotinylated secondary antibody at a 1:200 dilution (Dako, Denmark). Immunoreactions were visualized using diaminobenzidine hydrochloride (DAB Substrate Kit, Vector Laboratories) as chromogen. Sections were counterstained with haematoxylin as above. Images were obtained using an Olympus BX40 microscope (Olympus Imaging, Essex, UK) with Qcapture software (QImaging, Canada). Composite images of whole lungs were made from multiple single 100x images using Adobe Photoshop CS (Adobe Systems Inc, California, USA). Tumors were sized by histology at the widest midpoint on H & E stained slides by Qcapture software rather than by MRI due to partial volume and susceptibility effects that can over estimate tumor size.

Results

Two models of lung metastasis representative of high and low tumor cell seeding were evaluated by eqMRI (Figure 1, experimental dosing plan). Animals in the high tumor cell seeding model were followed weekly longitudinally up until day 28, these animals appeared healthy and recovered well at all time points after imaging (n = 3). Animals receiving low tumor cell seeding, generating discrete tumor nodules were taken for histology as soon as they were identified by MRI (n = 3). Bioluminescence

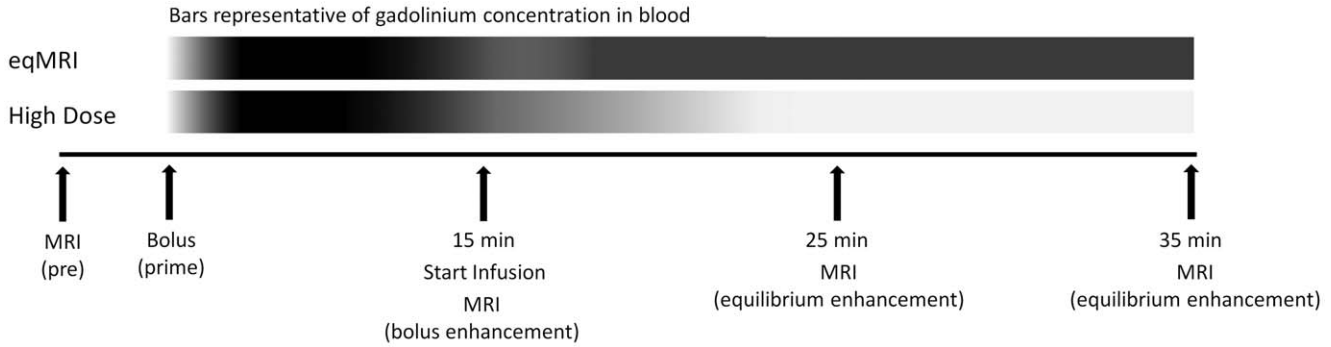

Figure 1. Experimental plan showing timings of bolus and infusion as well as scan times. The bars above are an assumed grey scale representation of gadolinium concentration within the blood where black is high and white low concentration.
doi:10.1371/journal.pone.0054903.g001

confirmed tumor growth in both models prior to identification by MRI (Figures S3 and S4). The SNR was used to assess the enhancement in individual tumors, while the increase in the volume of tumors becoming visible after Gd enhancement was expressed as the "percentage increase in observed tumors". Control lungs did not show any contrast enhancement throughout eqMRI (Figure 2A) (SNR was 1.68 ± 0.57 at pre contrast and constant throughout $p = 0.25$, $n = 3$).

Gd.DTPA Sustained at Equilibrium Improves the Detection of Pulmonary Tumors Compared to Bolus Enhancement

Lung metastases were detectable in animals receiving high tumor cell seeding as areas of hyperintensity from day 14, and from day 21 in low tumor cell seeding animals. eqMRI imaging defined two sets of tumors. Tumors visible on pre contrast images that did not change in presentation and their SNR values remained constant at all time points are termed as visible tumors (Figure 2 white arrowheads, Figure 3A). Tumors that only became visible with Gd enhancement at 15, 25 or 35 minutes but were not apparent on the pre scan image are termed enhancing tumors (Figure 2 white arrows). All high tumor cell seeding mice presented with multiple visible and enhancing tumors ($n = 9$ each). Whereas, low tumor cell seeding mice exhibited at least one visible ($n = 5$) and one enhancing tumor ($n = 3$) by MRI prior to histology. As the mice in the low tumor cell seeding model were taken as soon as tumors were visible by MRI for histology, this limited the numbers of tumors per mouse that could be assessed. Although the trends in Gd enhancement are similar for both models this needs to be taken into account. Also, the number of mice per group ($n = 3$) is a limiting factor when evaluating the percentage increase in observed tumor data.

Although a few diffuse tumors become evident at 15 minutes (Figure 2D 15 minutes, arrows) after the initial bolus prime, the majority of enhancing tumors were observed due to sustaining Gd equilibrium at 25 minutes onwards (Figure 2B and D, arrows). This is also evident in the rise in SNR in individual tumors from pre contrast compared to 15 minutes ($p = <0.05$) with a further increase at 25 minutes which was sustained at 35 minutes ($p = <0.05$) (Figure 3B and Figure S5B). eqMRI resulted in an significant increase in the percentage observed tumors at Gd equilibrium compared to bolus ($p = <0.05$) (Figure 3C and Figure S5C). Although in the low tumor cell seeding model there is an increase in the percentage observed tumors at 35 minutes compared to 25 minutes (Figure 3C), for the high tumor cell seeding model there is a reduction at 35 minutes compared to 25 minutes (Figure 4C & Figure S5C). This is most likely due to the amount of Gd accumulating within the tumors leading to susceptibility artefacts and T_2* affects, which is more apparent in high tumor cell seeding model.

Gd.DTPA at Equilibrium not the Dose Improves Pulmonary Tumor Detection

When a bolus dose of Gd.DTPA equivalent to the total dose of Gd.DTPA used in eqMRI was given as single bolus, animals did

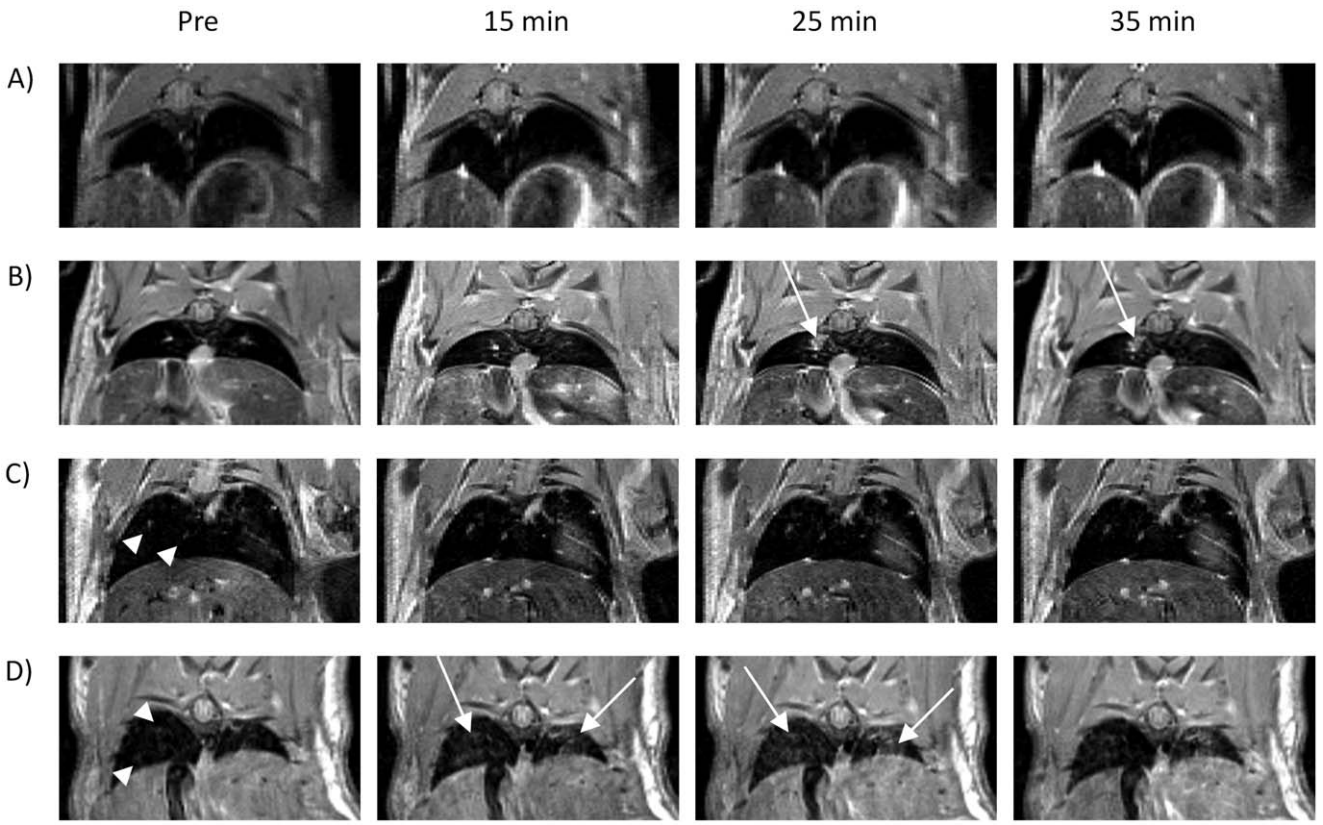

Figure 2. MR images over the 35 minute eqMRI time course. A) control lungs, B) a discrete gadolinium enhancing tumor nodule (25 minutes) (low tumor cell seeding model), C) tumor nodules visible on the pre contrast scan (low tumor cell seeding model), D) tumor presentation representative of a high tumor cell seeding model lung at day 14. Tumors visible on pre contrast (white arrowheads) and tumors only visible with gadolinium enhancement (white arrows) are indicated.
doi:10.1371/journal.pone.0054903.g002

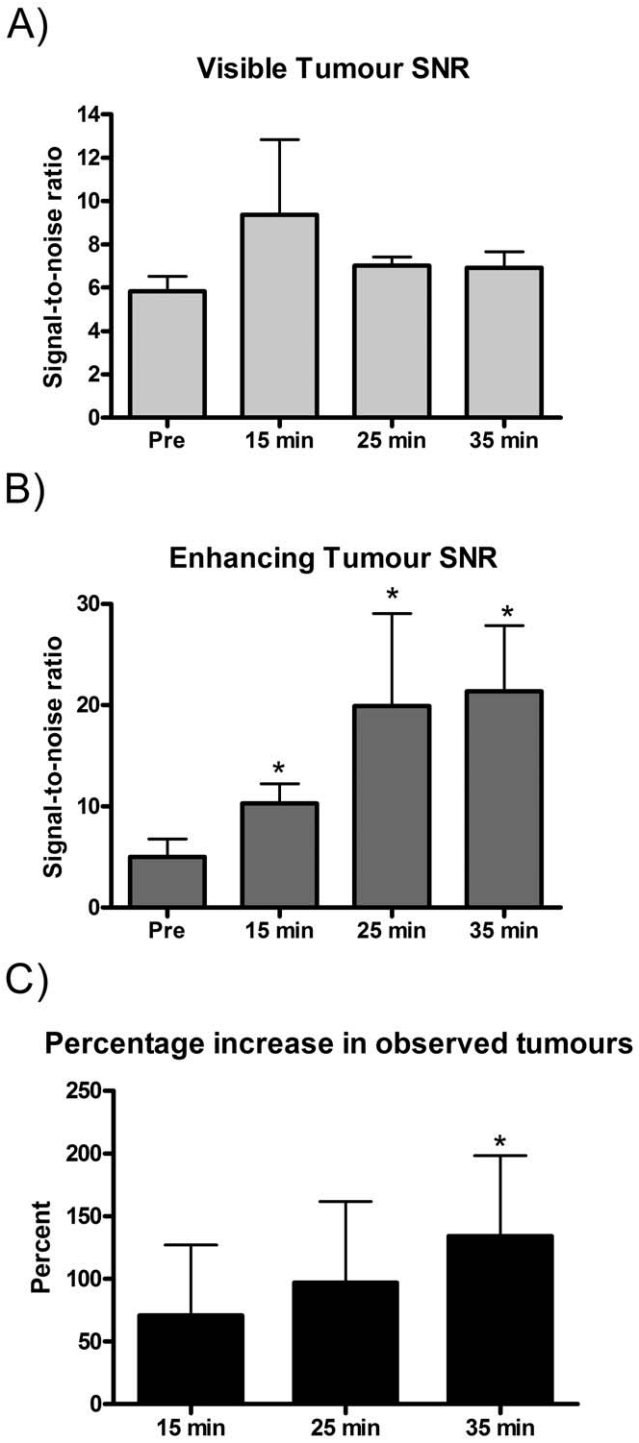

Figure 3. Low tumor cell seeding model mean values for signal-to noise (SNR) and the percentage increase in observed tumours for eqMRI. A) SNR of tumors already visible on pre contrast images, B) SNR of tumors that were visible due to Gd enhancement from 15 minutes onwards, C) the percentage increase in observed tumors by Gd enhancement at each time point compared to pre contrast. Values are mean ± s.e.m. * $p = <0.05$ from pre (A and B) or from 15 min (C).
doi:10.1371/journal.pone.0054903.g003

not present late enhancing tumors at 25 or 35 minutes (Figure 4A). Tumors visible on the pre contrast remained unchanged as in eqMRI (Figure 4A, white arrows). The percentage increase in observed tumors for both eqMRI and high dose Gd.DTPA was the same at 15 minutes (Figure 4B). Although, the high dose would be expected to increase the percentage observed tumors compared to the lower dose used in eqMRI at this time point, there appears to be no effect. This may be due to intergroup heterogeneity, but as fewer enhancing tumors appear to be present in the high dose this may indicate that any enhancing tumors are saturated with Gd causing susceptibility and T_2* effects as described previously affecting visualization. As the bolus has a limited time window for enhancement compared to Gd at equilibrium there is no further enhancement at 25 and 35 minutes for the high dose and the percentage increase in observed tumors is therefore significantly higher for eqMRI than the high bolus dose at these time points, confirming the contribution of Gd equilibrium to lung tumor enhancement (Figure 4B).

Gd Equilibrium Enhancing Tumors are Sub-millimeter in Size

Histology examination of lung sections corresponding to MR images for low tumor cell seeding mice, showed that tumors enhancing at 25 minutes onwards due to Gd equilibrium were sub-millimeter (<0.7 mm^2) tumors (Figure 5A), whereas tumors visible on pre contrast images tended to be larger (Figure 5B). Occasionally, visible tumors were also sub-millimeter in size and histology showed these as solid tumors (Figure 5D and E). Enhancing tumors however, appeared to line and fill the avelolar spaces with similar morphology to that shown by early bronchoavelolar cell carcinomas and atypical adenomatous hyperplasia (Figure 5C). Longitudinal evaluation of enhancing tumors showed that with tumor growth they become visible on the pre contrast scan further confirming them as tumors (Figure S6 white arrow at day 14 and subsequent white arrow head at day 21).

Discussion

In this study, primed infusions with a delay in equilibrium (eqMRI) of Gd.DTPA were used to compare gadolinium tumor enhancement of pulmonary tumors after bolus (as routinely used in the clinic), or gadolinium maintained at equilibrium. The results show that the maximal enhancement of pulmonary tumors was due to sustained Gd enhancement afforded by Gd equilibrium (25 minutes onwards) in both lung metastasis models. As few tumors enhanced after the high dose bolus prime (15 minutes), without Gd equilibrium the majority of enhancing tumors in this study would have been missed with a traditional Gd bolus MRI protocol.

Histological examination confirmed that the Gd equilbrium enhancing tumors were small (<0.7 mm) disorganised tumors with a low cellularity. The tumor cells line and fill the avelolar spaces in a similar manner to early bronchoavelolar cell carcinomas. The low cellular density means that they are not evident on the pre contrast scan and as the tumors are integrated within the avelolar spaces this increases the degree of diffusion of Gd.DTPA into the tumor interstitial spaces [31,32,33,34]. Gd equilibrium is therefore able to increase the concentration of Gd sufficiently, making them visible by MRI.

Both lung metastasis models presented with tumors that were already visible on pre contrast images. These tumors showed no significant contrast enhancement with Gd. Although, histological examination showed that they are generally larger than enhancing tumors, visible tumors could still be sub-millimeter in size. The

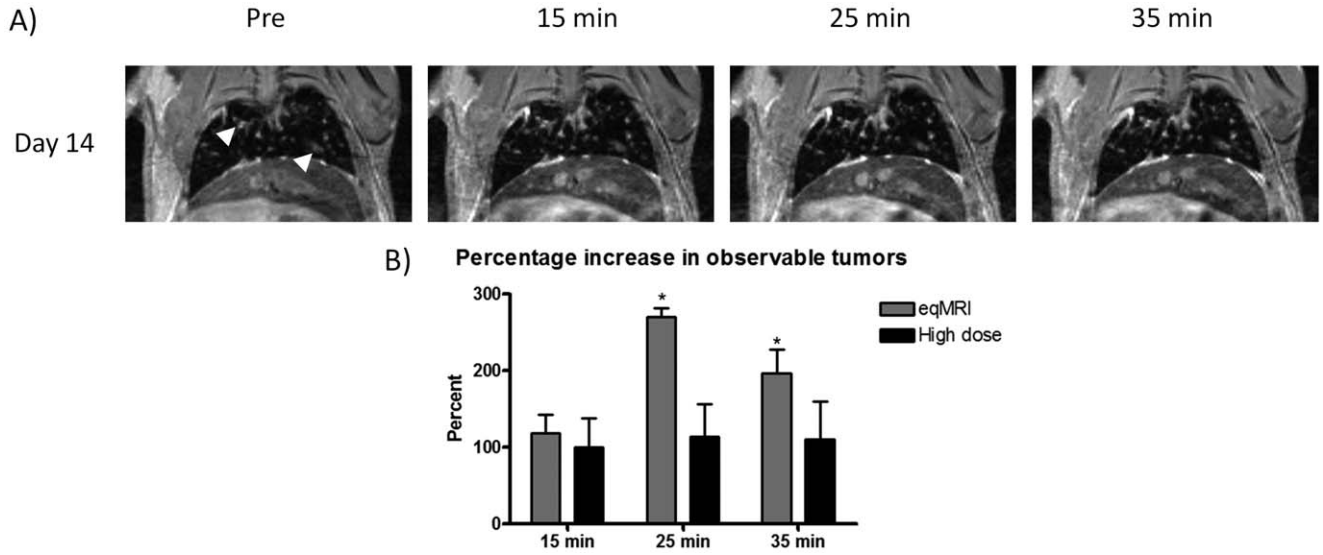

Figure 4. MR images of a high tumor cell seeding model mouse at day 14 over the 35 minutes for high dose Gd.DTPA (white arrowsheads denote visible tumors) (A), and the corresponding mean values for the percentage increase in observable tumors compared to that of high tumor cell seeding mice at day 14 for eqMRI (B). Values are mean ± s.e.m. * p = <0.05 from high dose.
doi:10.1371/journal.pone.0054903.g004

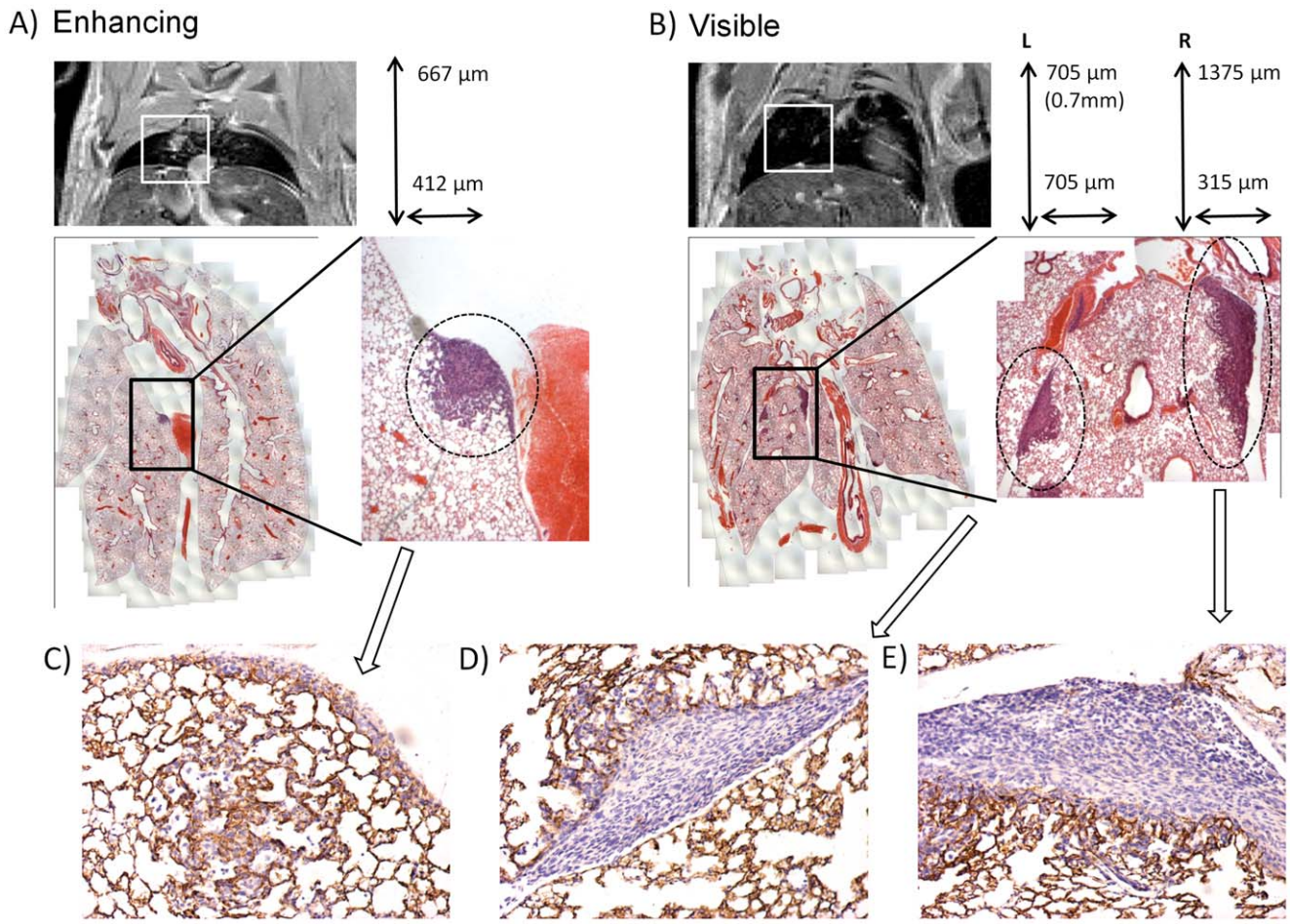

Figure 5. An MR image of a low tumor cell seeding model mouse lung the corresponding whole lung composite H & E stained section, a blown up area and sizing of tumor (white box), and CD34 immunohistochemistry image. A) a single enhancing tumour (at 25 minutes) with corresponding CD34 image (C), B) two visible tumors (pre contrast image) with corresponding CD34 images left (D) and right (E).
doi:10.1371/journal.pone.0054903.g005

main difference, except for size, appears to be that they have a higher cell density than the enhancing tumors, which may account for the early visualisation on MRI.

A previous study by Garbow *et al.* used a similar breathing gated sequence and detected lung tumor nodules in mice at a comparable size to the small visible tumors shown in this study [35]. Although the study did not investigate Gd enhancement, it verifies the use of MRI in the detection of sub-millimetre metastases. Other methods for lung metastasis imaging utilizing MRI such as Ultra-short echo time (UTE) imaging [36,37,38,39], fluorinated [40] or paramagnetic molecular oxygen [41] and most recently hyperpolarised ^{129}Xe and ^{3}H gas [42,43,44,45] have also been developed. A recent study by Branca *et al.* has combined hyperpolarized gas with tumor targeted iron oxide particles enhancing the detection of tumors at sub-millimetre sizes [46].

The gadolinium doses used in this study have been designed for the preclinical identification of small pulmonary metastases in mouse models of lung metastasis due to Gd given as a bolus or Gd maintained at equilibrium. The doses are therefore much higher than what would be used in the clinic. Although, this is a limitation, gadolinium can be maintained at equilibrium in humans at much lower doses and eqMRI has already been utilized in humans to assess myocardial fibrosis [25]. Although the use of this dosing regimen for the imaging of small pulmonary tumors would require further optimization, this methodology has the potential to be a safe and sensitive method for the detection of small primary or metastatic tumors in a similar fashion to CT. The dynamic uptake of Gd-chelates has been shown to improve the discrimination of benign and malignant tumors in other tissues types screening [47]. However, this has not been assessed in this study using eqMRI.

In conclusion, the results for this study demonstrate that a high concentration of sustained Gd enhancement afforded by eqMRI greatly improves the detection of sub-millimetre pulmonary metastases. The diffusion of contrast throughout the tumor mass increases the concentration of Gd retained causing enhancement when Gd equilibrium is reached.

Supporting Information

Figure S1 Flow diagram describing how the two sets of tumors were defined and how regions of interests where placed for individual tumor signal-to-noise calculations (see MRI data analysis). Drawn ROIs are only representative for explanation purposes.
(TIF)

Figure S2 Flow diagram describing how tumor volumes were calculated to assess the percentage increase in observed tumors due to Gd enhancement (see MRI data analysis).
(TIF)

Figure S3 Bioluminescent images of a high tumor cell seeding model mouse directly after infusion and at days 7 and 14 (A) and the corresponding plot of increasing bioluminescent signal (B) consistent with tumor growth.
(TIF)

Figure S4 Bioluminescent images of a low tumor cell seeding model mouse directly after infusion and weekly to 35 days (A) and the corresponding plot of increasing bioluminescent signal (B) consistent with tumor growth.
(TIF)

Figure S5 High tumor cell seeding model weekly mean values for signal-to noise (SNR) and the percentage increase in observed tumours for eqMRI. A) SNR of tumors already visible on pre contrast images, B) SNR of tumors that were visible due to Gd enhancement from 15 minutes onwards, C) the percentage increase in observed tumors by Gd enhancement at each time point compared to pre contrast. Values are mean ± s.e.m. * $p = <0.05$ from pre (A and B) or from 15 min (C).
(TIF)

Figure S6 MR images over the 35 minute eqMRI time course for a high tumor cell seeding model mouse at day 14 (top row), and day 21 (bottom row). Tumors that enhance due to gadolinium equilibrium (white arrow) at day 14, subsequently due to tumor growth are then visible on the pre contrast image (white arrowheads) at day 21.
(TIF)

Author Contributions

Conceived and designed the experiments: TLK AEC-W BMS ANP SW-S SMJ MFL. Performed the experiments: TLK AEC-W ES KLO. Analyzed the data: TLK AEC-W MFL. Contributed reagents/materials/analysis tools: TLK ES BMS ANP SW-S. Wrote the paper: TLK SMJ MFL.

References

1. Melamed MR, Flehinger BJ, Zaman MB, Heelan RT, Perchick WA, et al. (1984) Screening for early lung cancer. Results of the Memorial Sloan-Kettering study in New York. Chest 86: 44–53.
2. Frost JK, Ball WC Jr, Levin ML, Tockman MS, Baker RR, et al. (1984) Early lung cancer detection: results of the initial (prevalence) radiologic and cytologic screening in the Johns Hopkins study. Am Rev Respir Dis 130: 549–554.
3. Fontana RS, Sanderson DR, Taylor WF, Woolner LB, Miller WE, et al. (1984) Early lung cancer detection: results of the initial (prevalence) radiologic and cytologic screening in the Mayo Clinic study. Am Rev Respir Dis 130: 561–565.
4. Gohagan JK, Marcus PM, Fagerstrom RM, Pinsky PF, Kramer BS, et al. (2005) Final results of the Lung Screening Study, a randomized feasibility study of spiral CT versus chest X-ray screening for lung cancer. Lung Cancer 47: 9–15.
5. Aberle DR, Adams AM, Berg CD, Black WC, Clapp JD, et al. (2011) Reduced lung-cancer mortality with low-dose computed tomographic screening. N Engl J Med 365: 395–409.
6. Spiro SG, Navani N (2012) Screening for lung cancer: is this the way forward? Respirology 17: 237–246.
7. Kennel SJ, Davis IA, Branning J, Pan H, Kabalka GW, et al. (2000) High resolution computed tomography and MRI for monitoring lung tumor growth in mice undergoing radioimmunotherapy: correlation with histology. Med Phys 27: 1101–1107.
8. Patz EF, Jr., Black WC, Goodman PC (2001) CT screening for lung cancer: not ready for routine practice. Radiology 221: 587–591; discussion 598–589.
9. Kubota K, Matsuzawa T, Fujiwara T, Ito M, Hatazawa J, et al. (1990) Differential diagnosis of lung tumor with positron emission tomography: a prospective study. J Nucl Med 31: 1927–1932.
10. Gupta NC, Frank AR, Dewan NA, Redepenning LS, Rothberg ML, et al. (1992) Solitary pulmonary nodules: detection of malignancy with PET with 2-[F-18]-fluoro-2-deoxy-D-glucose. Radiology 184: 441–444.
11. Hoekstra CJ, Stroobants SG, Smit EF, Vansteenkiste J, van Tinteren H, et al. (2005) Prognostic relevance of response evaluation using [18F]-2-fluoro-2-deoxy-D-glucose positron emission tomography in patients with locally advanced non-small-cell lung cancer. J Clin Oncol 23: 8362–8370.
12. Song JW, Oh YM, Shim TS, Kim WS, Ryu JS, et al. (2009) Efficacy comparison between (18)F-FDG PET/CT and bone scintigraphy in detecting bony metastases of non-small-cell lung cancer. Lung Cancer 65: 333–338.
13. Gambhir SS (2002) Molecular imaging of cancer with positron emission tomography. Nat Rev Cancer 2: 683–693.
14. Gould MK, Fletcher J, Iannettoni MD, Lynch WR, Midthun DE, et al. (2007) Evaluation of patients with pulmonary nodules: when is it lung cancer?: ACCP evidence-based clinical practice guidelines (2nd edition). Chest 132: 108S–130S.
15. Weissleder R (2002) Scaling down imaging: molecular mapping of cancer in mice. Nat Rev Cancer 2: 11–18.
16. Runge VM, Wood ML (1988) Fast imaging and other motion artifact reduction schemes: a pictorial overview. Magn Reson Imaging 6: 595–607.

17. Hatabu H, Alsop DC, Listerud J, Bonnet M, Gefter WB (1999) T2* and proton density measurement of normal human lung parenchyma using submillisecond echo time gradient echo magnetic resonance imaging. Eur J Radiol 29: 245–252.
18. Semelka RC, Helmberger TK (2001) Contrast agents for MR imaging of the liver. Radiology 218: 27–38.
19. Padhani AR, Husband JE (2001) Dynamic contrast-enhanced MRI studies in oncology with an emphasis on quantification, validation and human studies. Clin Radiol 56: 607–620.
20. Fukumura D, Yuan F, Monsky WL, Chen Y, Jain RK (1997) Effect of host microenvironment on the microcirculation of human colon adenocarcinoma. Am J Pathol 151: 679–688.
21. Iyer AK, Khaled G, Fang J, Maeda H (2006) Exploiting the enhanced permeability and retention effect for tumor targeting. Drug Discov Today 11: 812–818.
22. Padhani AR (1999) Dynamic contrast-enhanced MRI studies in human tumours. Br J Radiol 72: 427–431.
23. Tofts PS, Berkowitz BA (1994) Measurement of capillary permeability from the Gd enhancement curve: a comparison of bolus and constant infusion injection methods. Magn Reson Imaging 12: 81–91.
24. Parker GJM, Clark D, Watson Y, Buckley DL, Berrisford C, et al. (2003) T1-Weighted DCE-MRI Apllied to Lung Tumours: Pre-Processing and Modelling. Proceedings of the 11th ISMRM Toronto: 1255.
25. Flett AS, Hayward MP, Ashworth MT, Hansen MS, Taylor AM, et al. (2010) Equilibrium contrast cardiovascular magnetic resonance for the measurement of diffuse myocardial fibrosis: preliminary validation in humans. Circulation 122: 138–144.
26. Campbell AE, Price AN, Ellmerich S, Simons P, Al-Shawi R, et al. (2011) Equilibrium contrast CMR for the detection of amyloidosis in mice. JCMR 13(S1): O60.
27. Zufferey R, Nagy D, Mandel RJ, Naldini L, Trono D (1997) Multiply attenuated lentiviral vector achieves efficient gene delivery in vivo. Nat Biotechnol 15: 871–875.
28. Price AN, Cheung KK, Lim SY, Yellon DM, Hausenloy DJ, et al. (2011) Rapid assessment of myocardial infarct size in rodents using multi-slice inversion recovery late gadolinium enhancement CMR at 9.4T. J Cardiovasc Magn Reson 13: 44.
29. Tidwell VK, Garbow JR, Krupnick AS, Engelbach JA, Nehorai A (2012) Quantitative analysis of tumor burden in mouse lung via MRI. Magn Reson Med 67: 572–579.
30. Aguilar S, Scotton CJ, McNulty K, Nye E, Stamp G, et al. (2009) Bone marrow stem cells expressing keratinocyte growth factor via an inducible lentivirus protects against bleomycin-induced pulmonary fibrosis. PLoS One 4: e8013.
31. Vaupel P, Kallinowski F, Okunieff P (1989) Blood flow, oxygen and nutrient supply, and metabolic microenvironment of human tumors: a review. Cancer Res 49: 6449–6465.
32. Fleming JB, Brekken RA (2003) Functional imaging of angiogenesis in an orthotopic model of pancreatic cancer. J Cell Biochem 90: 492–501.
33. Bergers G, Benjamin LE (2003) Tumorigenesis and the angiogenic switch. Nat Rev Cancer 3: 401–410.
34. Jain RK (2005) Antiangiogenic therapy for cancer: current and emerging concepts. Oncology (Williston Park) 19: 7–16.
35. Garbow JR, Zhang Z, You M (2004) Detection of primary lung tumors in rodents by magnetic resonance imaging. Cancer Res 64: 2740–2742.
36. Hatabu H, Chen Q, Stock KW, Gefter WB, Itoh H (1999) Fast magnetic resonance imaging of the lung. Eur J Radiol 29: 114–132.
37. Togao O, Tsuji R, Ohno Y, Dimitrov I, Takahashi M (2010) Ultrashort echo time (UTE) MRI of the lung: assessment of tissue density in the lung parenchyma. Magn Reson Med 64: 1491–1498.
38. Takahashi M, Togao O, Obara M, van Cauteren M, Ohno Y, et al. (2010) Ultra-short echo time (UTE) MR imaging of the lung: comparison between normal and emphysematous lungs in mutant mice. J Magn Reson Imaging 32: 326–333.
39. Kokuryo D, Kumamoto E, Takao Y, Fujii S, Kaihara T, et al. (2012) Evaluation of a vessel-tracking-based technique for dynamic targeting in human liver. Magn Reson Med 67: 156–163.
40. Rinck PA, Petersen SB, Lauterbur PC (1984) [NMR imaging of fluorine-containing substances. 19-Fluorine ventilation and perfusion studies]. Rofo 140: 239–243.
41. Edelman RR, Hatabu H, Tadamura E, Li W, Prasad PV (1996) Noninvasive assessment of regional ventilation in the human lung using oxygen-enhanced magnetic resonance imaging. Nat Med 2: 1236–1239.
42. Albert MS, Cates GD, Driehuys B, Happer W, Saam B, et al. (1994) Biological magnetic resonance imaging using laser-polarized 129Xe. Nature 370: 199–201.
43. Saam BT, Yablonskiy DA, Kodibagkar VD, Leawoods JC, Gierada DS, et al. (2000) MR imaging of diffusion of (3)He gas in healthy and diseased lungs. Magn Reson Med 44: 174–179.
44. Salerno M, Altes TA, Mugler JP 3rd, Nakatsu M, Hatabu H, et al. (2001) Hyperpolarized noble gas MR imaging of the lung: potential clinical applications. Eur J Radiol 40: 33–44.
45. Driehuys B, Hedlund LW (2007) Imaging techniques for small animal models of pulmonary disease: MR microscopy. Toxicol Pathol 35: 49–58.
46. Branca RT, Cleveland ZI, Fubara B, Kumar CS, Maronpot RR, et al. (2010) Molecular MRI for sensitive and specific detection of lung metastases. Proc Natl Acad Sci U S A 107: 3693–3697.
47. Fan X, Medved M, River JN, Zamora M, Corot C, et al. (2004) New model for analysis of dynamic contrast-enhanced MRI data distinguishes metastatic from nonmetastatic transplanted rodent prostate tumors. Magn Reson Med 51: 487–494.